Bootstrapping and Resetting CMOS Starter for Thermoelectric and Photovoltaic Chargers

Andrés A. Blanco, *Graduate Student Member, IEEE*, Gabriel A. Rincón-Mora, *Fellow, IEEE*

***Abstract*—Sustaining microsensors for years is challenging because tiny batteries exhaust quickly, and recharging or replacing thousands of networked nodes is impracticable. Harnessing heat or light energy helps, but only when available. And even then, tiny generators output less than 300 mV, which is not enough to operate microelectronics well. This paper presents a 0.18-µm CMOS starter that charges a temporary 1.8-V supply quickly and reliably from slow- or fast-rising photovoltaic and thermoelectric sources. For this, a jump starter helps an LC tank oscillate to a level that allows a discharge path to output power. A resetter then continually resets the circuit until the system senses the temporary supply is ready. This way, with 1.8 V, a charging system can then charge a battery quickly before the onset of another harvesting drought. The starter does not require off-chip components because it borrows the switched inductor that the charging system already uses to charge the battery. A prototype of the starter proposed charges 120 pF to 1.8 V in 15–59 µs with 1.5%–7% efficiency from a 180-Ω, 220–250-mV source.**

***Index Terms*—Heat and light energy harvester, thermoelectric, photovoltaic, dc-sourced starter, switched-inductor charger.**

I. Starting DC-Sourced Energy-Harvesting Chargers

Wireless microsensors can add cost-, energy-, and life-saving intelligence to remote and inaccessible places in engines, vehicles, homes, hospitals, airplanes, office buildings, factories, ships, space stations, and the human body [1]–[4]. Their usefulness hinges on tiny dimensions and wireless operation. Small batteries, however, drain quickly. And periodically recharging thousands of nodes across a wide network is impracticable. Luckily, heat and light energy are often available. Harvesting power from these sources can continually replenish a battery that drains easily.

Still, ambient sources can vanish [5] long enough for onboard batteries to deplete. Energy-harvesting microsystems must therefore wake often, and long enough to perform tasks before another drought begins. The battery must, as a result, charge quickly. But when the source v_S outputs 200–400 mV, which is what mm transducers generate with 20°–25° C [6] or indoor lighting [7]–[8], chargers output less than 1% of the power they harvest. With so little power, the charger requires seconds to charge the battery [9]. Stacking cells is possible, but not without a substantial loss in drawn power [10].

The starter in Fig. 1 accelerates this wake time by charging a smaller, but higher-voltage temporary supply v_T that feeds the charger. Once the temporary supply is ready, the charger sends an off signal that disables the starter. This way, with 1–2 V, the charger can output with P_{CHG} 80%–90% of the power it harvests with P_H [11]. With so much more power, the battery C_B can charge in milliseconds or less.

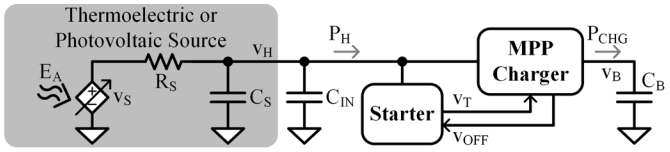

Fig. 1. Thermoelectric energy-harvesting charger system.

In practice, the intensity of the ambient source varies, which means v_S changes over time. Thermoelectric generators and photovoltaic cells also incorporate a series resistance R_S that consumes power. So to output maximum power, the charger should draw just enough power to keep the harvested source v_H near its maximum power point (MPP) [3], [6], [12]. But since switched inductors draw alternating current, the system includes a capacitor C_{IN} that suppresses variations in v_H.

This paper presents a bootstrapping and resetting starter that charges a temporary supply in microseconds from slow- and fast-ramping resistive millivolt dc sources. Sections II and III describe and discuss the operation and performance of the prototyped implementation. Sections IV and V then assess performance and summarize conclusions.

II. Proposed Bootstrapping and Resetting Starter

The switched inductor in Fig. 2 implements an oscillating core that energizes and drains L_X from a dc source v_S into a temporary supply C_T. The jump starter bootstraps the circuit so oscillations that start from a low harvesting voltage v_H can activate the oscillating core. The resetter restarts the oscillating core until the temporary supply reaches its target.

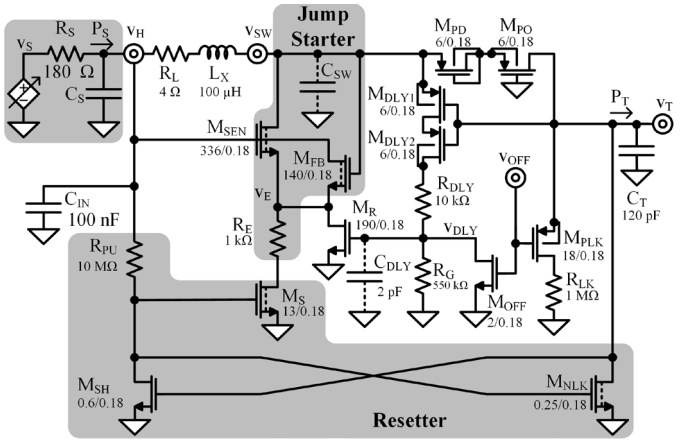

Fig. 2. 0.18-µm bootstrapped oscillating starter.

Manuscript received on October X, 2016; revised on Month X, 2017; and accepted on Month X, 2017. The authors thank Paul Emerson, Dr. Rajarshi Mukhopadhyay, Dr. Orlando Lazaro, and Texas Instruments for their support, advice, and sponsorship.

The authors are with the School of Electrical and Computer Engineering at the Georgia Institute of Technology, Atlanta, GA 30332-0250 U.S.A. E-mail: ablanco@gatech.edu, Rincon-Mora@gatech.edu.

A. Oscillating Core

When v_H is at or above $v_{H(MIN)}$, the gate voltage of low-threshold switch M_{SEN} is high enough for M_{SEN} to draw current i_L through L_X into R_E. This energizes L_X from v_S. But as i_L ramps (past 14.7238 ms in Fig. 3), R_E's voltage v_E climbs and collapses M_{SEN}'s gate–source voltage. So M_{SEN} opens and i_L flows into C_{SW} to charge C_{SW} to v_H, which ends the energizing period t_E. With current energy still in L_X, L_X then drains into C_{SW} to raise v_{SW} above v_H. If v_{SW} rises two threshold voltages $2|v_{TP}|$ above C_T's v_T: above $v_{SW(MIN)}$, diode and ground switches M_{PD} and M_{PO} close to deplete L_X into C_T.

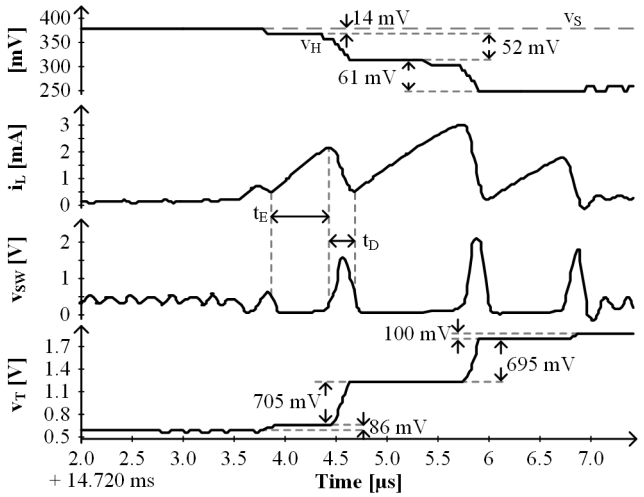

Fig. 3. Measured oscillating and charging waveforms.

To charge C_T quickly, L_X should draw and deliver as much $0.5L_Xi_L^2$ energy as possible. But to keep i_L from burning too much ohmic power, L_X should be high. With 100 µH, C_{SW} charges 1.5 V and C_T 705 mV as L_X drains across t_D in Fig. 3.

When v_{SW} is high enough above C_T's v_T, M_{DLY1} and M_{DLY2} close to steer some of i_L into C_{DLY}. With sufficient energy, C_{DLY} charges enough to close M_R and re-engage M_{SEN}, and in so doing, drain C_{SW}. v_{SW} therefore drops, and when v_{SW} falls below v_H, L_X begins to energize and start another cycle. But since C_{DLY} and R_G keep M_R engaged for t_G, L_X energizes that much longer on the second cycle to peak i_L to a higher level.

Notice C_{DLY} does not begin to charge until v_{SW} rises above v_T by $|v_{TP}|$. And C_{DLY} does not trip M_R until after R_{DLY}'s delay t_{DLY}. After v_{SW} falls and R_G's delay t_G, R_G resets M_R's gate to zero. Like in [13], t_{DLY} should be long enough to ensure C_T receives energy from L_X, but also shorter than t_D. And t_G should be shorter than t_E. Expressions for these in [13] specify their limits and simulations confirm that C_T charges to 1.4 V from 220 mV when R_{DLY}, R_G, and C_{DLY} vary –50% to +100%.

M_{PD}–M_{PO}'s and M_{DLY1}–M_{DLY2}'s body diodes are head-to-head and back-to-back to block one another as v_{SW} rises to $v_{SW(MIN)}$. This is important because leaking energy away from C_{SW} can keep v_{SW} from reaching its minimum threshold. M_{PO} keeps $v_{SW(MIN)}$ from dropping below $2|v_{TP}|$ to ensure v_{SW} is high enough to charge C_{DLY} and re-engage M_{SEN}. As v_T rises, M_{PO} drops a lower voltage, and as a result, burns less power.

B. Jump Starter

For the core to oscillate, v_{SW} must climb $|v_{TP}|$ above v_T to close M_{DLY1} and M_{DLY2}. v_S and L_X must therefore charge C_{SW} above this $|v_{TP}| + v_T$ threshold $v_{SW(MIN)}$. But in addition to C_{SW}'s $0.5C_{SW}(|v_{TP}| + v_T)^2$, v_S and L_X must also supply M_{SEN}'s leakage and v_S's and L_X's ohmic losses in R_S and R_L. For this, L_X must first draw enough energy E_L from v_S. Since E_L climbs with v_H, v_H must similarly surpass a threshold $v_{H(MIN)}$. So to keep $v_{H(MIN)}$ low, L_X and M_{SEN}'s off resistance should be high and C_{SW}, $|v_{TP}|$, R_S, R_L, v_T, and M_{SEN}'s on resistance low.

Although M_{SEN}'s current falls as v_E rises, M_{SEN} does not shut. So M_{SEN} leaks E_L energy away from C_{SW}. M_{FB} reduces this leakage because, as v_{SW} and v_E climb, M_{FB} shorts M_{SEN}'s gate–source terminals. C_{SW} therefore receives more of E_L and charges to $v_{SW(MIN)}$ with less energy. That way, a lower $v_{H(MIN)}$ can charge C_{SW} to $v_{SW(MIN)}$.

C. Resetter

Although L_X loads C_{IN}, v_S supplies much of the current that L_X draws when energizing at 3.8–4.4 µs in Fig. 3, so v_H falls, but not by much. When L_X drains at 4.4–4.7 µs, however, M_{FB} closes and pulls additional current from C_{IN}. This is why C_{IN} discharges and v_H falls more at 4.4–4.7 µs than at 3.8–4.4 µs. The challenge with v_H falling is that v_T rises after L_X delivers a packet to C_T, so v_{SW} must climb to a higher threshold $v_{SW(MIN)}$. In other words, $v_{H(MIN)}$ increases with every cycle. And if v_H falls below $v_{H(MIN)}$ after one cycle, v_H may not be high enough to reach the higher $v_{H(MIN)}$. This can stall the circuit.

To fix this runaway problem, the starter can repeat the startup process until C_T receives enough energy to supply the charger in Fig. 1. For this, M_{SH} shuts the jump starter (by opening M_S) each time C_T charges above M_{SH}'s threshold V_{TN0}. M_R, however, can still help L_X and C_{SW} oscillate and charge C_T. So if v_H does not fall below $v_{H(MIN)}$, like in Fig. 3, C_T can charge to its target in one or two more cycles.

If v_H falls below $v_{H(MIN)}$, the core stops oscillating. This removes the load that droops v_H, so v_H rises to v_S. Meanwhile, M_{PLK} discharges C_T, so $v_{H(MIN)}$ also falls. When v_T falls low enough below V_{TN0}, M_{SH} opens to close M_S and reactivate the jump starter. These attempts continue until v_H is high enough to charge C_T fully. At that point, the charger sends an off signal v_{OFF} that disables the oscillating core so it can no longer reset. $v_{H(MIN)}$ is therefore the voltage necessary to charge C_{SW} $|v_{TP}|$ above v_T's reset level V_{TN0} and C_T to its target from V_{TN0}.

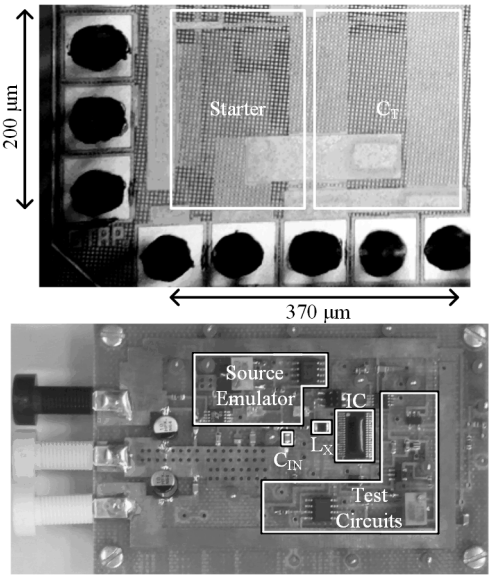

Fig. 4. Prototyped die and experimental board.

III. Measured Performance

The 200 × 370-μm^2 die in Fig. 4 integrates the bootstrapping and resetting 0.18-μm CMOS starter and the 120-pF temporary supply C_T in Fig. 2. The ambient source, transfer inductor L_X, and input capacitor C_{IN} are off chip. A 0–400-mV source v_S and a 180-Ω series resistor R_S emulate the thermoelectric source. The 100-μH inductor includes 4 Ω of series resistance and occupies 2 × 1.25 × 1.45 mm^3. The 100-nF capacitor includes 100 mΩ of series resistance and measures 1.6 × 0.8 × 0.6 mm^3. For testing purposes, the board also includes an off-chip comparator that monitors C_T's v_T to generate the off signal v_{OFF} that the charger in Fig. 1 outputs when v_T is high enough to operate the charger. Component values subscribe to the operating, low-loss, and low-footprint guidelines and principles described here and detailed in [13].

A. Startup

Off Phase: After a prolonged harvesting drought, the charger depletes the input capacitor C_{IN} and the load empties the battery C_B. So when ambient energy first raises v_S above ground, all nodes in the circuit are near ground. And as long as v_H remains below 180 mV in Fig. 5, nothing conducts current. So the starter is off and v_H follows v_S as v_S ramps up.

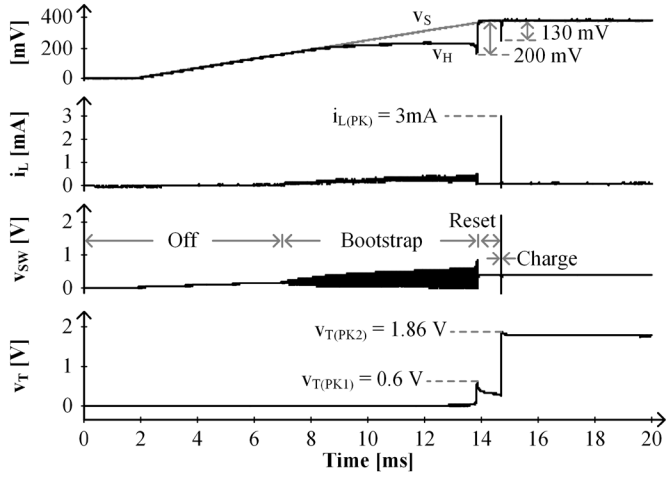

Fig. 5. Measured startup waveforms.

Bootstrap Phase: At and above 180 mV, M_{SEN} in the starter conducts enough current to energize L_X, but not enough for L_X to raise v_{SW} to $v_{SW(MIN)}$. Still, with the help of M_{FB}, L_X depletes into C_{SW} and C_{SW} drains back into L_X. And as v_H rises above 180 mV, L_X and C_{SW} exchange energy without drawing or delivering much power. As oscillations grow, however, more inductor power leaks into C_{DLY}. This loads the source, so that at about 9 ms, when v_S is 200 mV, v_H begins to droop below v_S. With v_H just below the minimum threshold $v_{H(MIN)}$, the jump starter continues to bootstrap v_{SW}, so oscillations grow and loading persists, but C_T still does not charge.

Reset Phase: When the energy leaked into C_{DLY} is sufficiently high to engage M_R in Fig. 2, the oscillating core begins to operate. So at 13.8 ms in Fig. 5, L_X draws considerably more energy from v_S than in the bootstrapping phase. As a result, v_H dips further and excess L_X energy charges C_T to 0.6 V. But since v_T is not high enough for the charger to operate and shut the starter, M_{SH} shuts the jump starter. M_{PLK} discharges C_T until M_{SH} again opens at 14.7 ms to reactivate the starter. Without a load, v_H is now high enough at v_S to charge C_T to 1.86 V. So at this point, the comparator that emulates the charger disables the starter.

B. Minimum Input Threshold

To determine the minimum level $v_{H(MIN)}$ above which the starter can charge C_T, the input source v_S in Fig. 6 should ramp at a rate that is much slower than the startup time t_{ST} of the system. This way, the impact of startup dynamics on measured readings is minimal. In the case of Fig. 6, rise time $t_{H(R)}$ is over 0.5 s. This value is orders of magnitude greater than the 15–135 μs that the starter requires to charge C_T. Measurements therefore demonstrate that the starter starts with 215–222 mV.

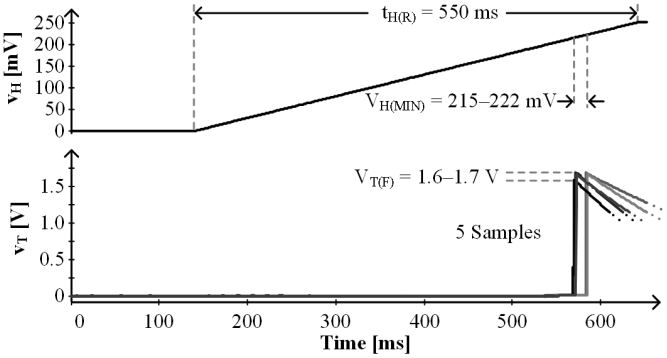

Fig. 6. Minimum input threshold measured.

C. Reliable Starts

The starter incorporates three oscillators that must start and interface reliably to charge the temporary supply C_T. More specifically, the jump starter should start and oscillate until v_{SW} is high enough to activate the oscillating core. The core must then oscillate and charge C_T. But if C_T does not reach the voltage the charger requires, the resetter must shut and reactivate the starter and oscillate this way until C_T does.

In the case of energy harvesters, ambient energy can vanish and reappear slowly. And in some cases, an external force or signal can suddenly inhibit and reconnect an ambient source. The system must therefore be able to start from slow- and fast-rising ramps. But to start, the input v_H must surpass the 215–222-mV minimum level $v_{H(MIN)}$ that the starter requires to operate. This is why v_H in Fig. 7 rises to 250 mV in 100 ns and 1, 5, and 10 ms. In all cases, the starter charges C_T to 1.8 V.

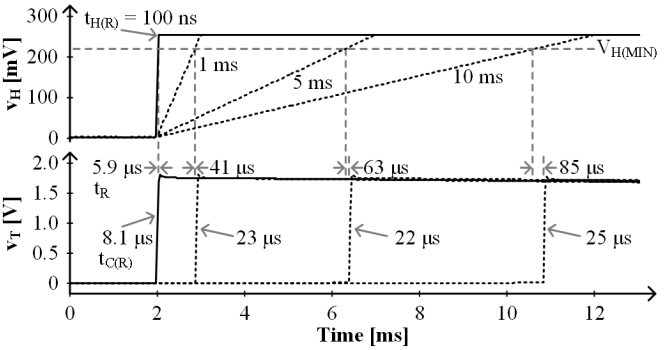

Fig. 7. Measured starts for 100 ns–10 ms input rise times.

D. Startup Time

Startup time t_{ST} is the time after v_H reaches $v_{H(MIN)}$ that the system requires to charge C_T to, in this case, 1.8 V. When v_H rises in $t_{H(R)}$ or 1, 5, and 10 ms in Fig. 7, for example, the

starter requires t_R or 41, 63, and 85 µs to react and $t_{C(R)}$ or 22–25 µs to charge C_T. So startup times t_{ST} are 64, 85, and 110 µs. Startup delay or response time t_R lengthens with $t_{H(R)}$ because v_H rises less quickly. So by the time C_T charges, v_H reaches a lower level. And with a lower overdrive voltage, the jump starter requires more time to activate the oscillating core.

Charge time $t_{C(R)}$ is consistent at 22–25 µs for 1-, 5-, and 10-ms rise times because v_H and the time t_E across which L_X energizes do not vary much. $t_{C(R)}$ is 66% shorter at 8 µs when $t_{H(R)}$ is 100 ns because v_H rises above the minimum threshold $v_{H(MIN)}$ before the starter can respond. As a result, the oscillating core energizes L_X without help from the resetter. In other words, $t_{C(R)}$ excludes reset delays.

When v_H rises to 220–250 mV in the same time span, across 100 ns, charge time $t_{C(R)}$ in Fig. 8 is fairly constant at 8 µs. This means, reset delays remain absent. Response times t_R, however, fall from 32–52 to 6–16 µs with ascending v_H levels, as v_H peaks increase from 220 to 250 mV. The culprit for this rise in t_R is the jump starter. This is because v_{SW} in Fig. 2 requires more time to bootstrap to $v_{SW(MIN)}$ when v_H is lower.

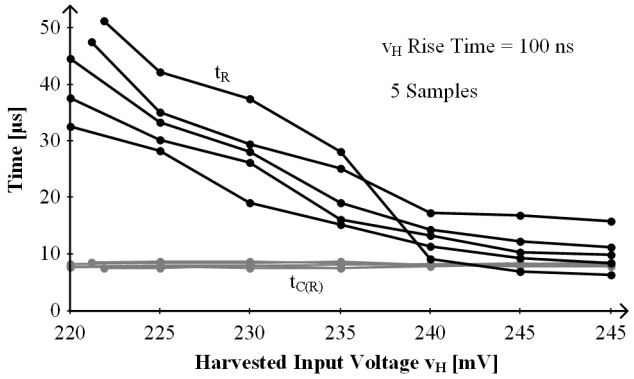

Fig. 8. Measured startup times after stepping the input.

E. Energy Management

Wake time for energy-harvesting microsensors is a critical parameter because ambient sources can vanish and reappear without notice. Charging systems should therefore charge a battery C_B quickly. And for that, C_B should receive as much power as possible. With the temporary supply C_T that the starter in Figs. 1 and 2 establish, the charger can do this: output 80%–90% of the power it harvests [11]. This is possible because v_T is high enough at 1.8 V, for example, to keep resistances in the network in the milliohm range.

Before C_B can receive power, however, the starter must charge C_T. But with only millivolts at the supply, starters do not have milliohm transistors with which to switch the inductor L_X. So transistors burn a large fraction of the power that could otherwise reach C_T. As a result, ohmic losses in the starter extend the time that C_T requires to charge.

In the case of the prototyped starter, M_{FB} in the jump starter and M_{SEN} in the energizing path in Fig. 2 burn the most energy across the charging process. M_{FB}'s loss is significant at 4.4–16 nJ when v_R rises to 235–300 mV in 100 ns in Fig. 9. This is because M_{FB} draws substantial current from the harvested input v_H every time v_{SW} rises (as L_X drains).

M_{SEN} dissipates the next highest loss at 0.6–1.2 nJ every time L_X energizes. The rest of the circuit consumes another 200 pJ. So in delivering 194 pJ to charge C_T's 120 pF to 1.8 V, the starter outputs 1.5%–7% of the power the ambient source supplies when v_H rises to 235–300 mV.

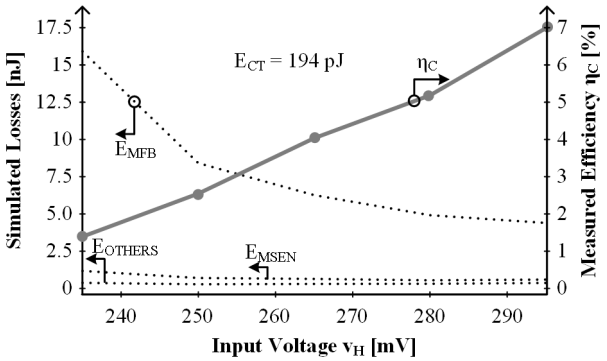

Fig. 9. Simulated losses and measured power efficiency.

IV. Relative Performance

Integration: Because microsensors are useful in many more applications when they are smaller, one critical parameter to consider is integration. In this case, the starter requires a 200 × 370-µm^2 0.18-µm die and a 2 × 1.25 × 1.45-mm^3 100-µm inductor. So combined, the starter occupies about 4 mm^3, which compares very favorably with [12], [6], and [14] and is competitive with [15] and [16] in Table I.

TABLE I: Performance Summary and the State of the Art

	X-Former [12]	MEMS Switch [6]	LC Osc. [14]	Ring Oscillator		LC Charger [13]	This Work
				Tuned [15]	Natural [16]		
$V_{H(MIN)}$	40 mV	35 mV	50 mV	80 mV	330 mV	300 mV	220 mV
C_{ST}	10 µF	470 pF	4.7 nF	30 pF	–	100 pF	120 pF
V_{TAR}	1.2 V	1 V	0.8 V	1.3 V	1.8 V	0.55 V	1.8 V
t_{ST}	4.9 s	3 ms	15 ms	4.8 ms	1.2 s	44 µs	59 µs
$^*I_{EQ}$	2.45 µA	157 nA	251 nA	8 nA	–	1.25 µA	3.66 µA
η_{ST}	–	–	–	–	–	0.5%	1.5% 7%
Other	1:60 X-Former	22 µH 22 µH MEMS Switch	2 µH 2 µH 100 µH 27 µH	6.8 µH	–	100 µH	100 µH
Vol.	175 mm^3	150 mm^3	**16 mm^3	**4 mm^3	4 mm^3	4 mm^3	4 mm^3
Tech.	0.13 µm	0.35 µm	65 nm	65 nm	–	0.18 µm	0.18 µm

*Equivalent $C_{ST}V_{TAR}/t_{ST}$ current. **Projected estimates based on availability.

[12] requires a transformer that, at 175 mm^3, occupies 38× more space than the 4 mm^3 required here. [6] uses a MEMS device that switches in response to vibrations. Relying on such a switch is a drawback because the charger can only start with motion. [6] also requires two inductors that, at 150 mm^3, occupy 38× more volume than the starter presented here. [14] is much better in both respects, but with four inductors, [14] still occupies 16 mm^3, which is 4× more space.

At 4 mm^3, [15] and [16] are comparable in size. The challenge with [15] is cost. Because to start from 80 mV, P- and N-type transistor threshold voltages in the ring oscillator that start the system must balance *specifically* for that purpose. So [15] requires post-processing steps in the fabrication process. These steps are costly and time consuming, and without them, the minimum threshold would be that of their less demanding siblings in [16]: 330 mV.

Capacitor and super capacitors receive and deliver power at any voltage across more than 500k recharge cycles [9]. Lithium- and nickel-based chemistries operate at higher voltages, so $v_{H(MIN)}$ can be higher and t_{ST} longer. But they can only recharge 1k–1.2k times [9]. Unfortunately, tiny devices can deplete so often that cycle life must be higher. So although this and others in Table I can charge many types of batteries, capacitors and super capacitors are more likely candidates.

Startup Time: Another equally important parameter is startup time t_{ST}. This is because each time the ambient source vanishes and reappears, t_{ST} determines if and what the sensor can accomplish. t_{ST}, however, changes with capacitance C_T and target voltage V_{TAR}, so comparing t_{ST} alone can be misleading. But since V_{TAR} and C_T will, for the most part, extend t_{ST} in the same way, equivalent C_TV_{TAR}/t_{ST} current I_{EQ} is a better figure of merit (FoM). From this perspective, I_{EQ} for the starter presented here is 3.66 µA, which is 23×, 15×, and 458× higher than [6], [14], and [15], and even without a transformer, still 50% higher than [12].

Minimum Threshold: More space, higher cost, and longer starts are the ultimate tradeoffs for lower input threshold $v_{H(MIN)}$ in [12], [6], [14], and [15]. $v_{H(MIN)}$ for these technologies is 35–80 mV, which is 16%–36% of the 220 mV that the circuit here requires. But if space and cost are critical constraints, which is the case for many emerging applications with wide-area networks, $v_{H(MIN)}$ is unfortunately a necessary sacrifice. This sacrifice, however, is 50% more severe for [16] at 330 mV than for the starter proposed here.

Predecessor: The starter here differs from its predecessor in [13] in three basic ways. First, the oscillator in [13] energizes L_X into a capacitor and the oscillating core here into a resistor R_E. Of the two, R_E establishes a higher voltage more quickly. M_{SEN} therefore shuts sooner and more effectively, and as a result, loses less energy. And although the capacitor receives charge it can hold, [13] nevertheless drains it to ground.

M_{FB} closes a bootstrapping positive feedback loop that is absent in [13]. This loop starts oscillating and bootstrapping the circuit from a lower input voltage. Plus, the starter incorporates a resetter that restarts the circuit until L_X can charge C_T fully. Without these improvements, [13] only starts when a non-resistive input rises in less than 300 ns, C_T's final voltage varies with input voltage, conversion efficiency is 3×–14× lower, and the minimum input threshold is 80 mV higher.

V. Conclusions

The 0.18-µm CMOS starter presented here charges 120 pF to 1.8 V in 15–59 µs with 1.5%–7% of the power it draws from a 180-Ω, 220–250-mV source. It is compact, low cost, and robust. For this, a jump starter bootstraps the input to a voltage that is high enough to activate an oscillating core that charges. A resetter then restarts the circuit until the temporary supply reaches its target. Charging a temporary supply this quickly is important, because with 1–2 V, a charger can deliver 80%–90% of the power it harvests. This way, the time required to charge both the smaller temporary supply and the larger battery is much faster than charging the larger battery alone with the less efficient starter. A wireless microsensor can therefore wakeup much quicker. And this way, the system can perform many more tasks in the brief time that an ambient source is strong enough to overcome losses and supply power.

References

[1] R. Vullers, *et al.*, "Energy Harvesting for Autonomous Wireless Sensor Networks," *IEEE Solid-State Circuits Magazine*, vol. 2, pp. 29–38, 2010.

[2] D.F. Lemmerhirt and K.D. Wise, "Chip-Scale Integrations of Data-Gathering Microsystems," *Proceedings of IEEE*, vol. 94, pp. 1138–1159, June 2006.

[3] Y. Lee, *et al.*, "A Modular 1 mm^3 Die-Stacked Sensing Platform with Low Power I^{2}C Inter-Die Communication and Mutli-Modal Energy Harvesting," *IEEE Journal of Solid-State Circuits*, vol. 48, pp. 229–243, January 2013.

[4] T. Kang, *et al.*, "An Energy Combiner for a Multi-Input Energy-Harvesting System," *IEEE Trans. on Circuits and Systems II*, vol. 62, pp. 911–915, September 2015.

[5] M.L. Ku, Y. Chen, and K.J.R. Liu, "Data-Driven Stochastic Models and Policies for Energy Harvesting Sensor Communications," *IEEE* J. on Selected Areas in Communications, vol. 33, pp. 1505–1520, August 2015.

[6] Y.K. Ramadass, *et al.*, "A Battery-Less Thermoelectric Energy Harvesting Interface Circuit with 35 mV Startup," *IEEE J. of Solid-State Circuits*, vol. 46, pp. 333–341, January 2011.

[7] R.D. Prabha and G.A. Rincón-Mora, "Drawing the Most Power From Low-Cost Single-Well 1-mm^2 CMOS Photovoltaic Cells," *IEEE Trans. on Circuits and Systems II*, vol. 64, pp. 46–50, January 2017.

[8] G. M. Pour, M. Benyhesan, and W. D. Leon-Salas, "Energy Harvesting Using Substrate Photodiodes," *IEEE Trans. on Circuits and Systems II*, vol. 61, pp. 501–505, July 2014.

[9] H. Yang and Y. Zhang, "Analysis of Supercapacitor Energy Loss for Power Management in Environmentally Powered Wireless Sensor Nodes", *IEEE Trans. on Power Electronics*, vol. 28, pp. 5391-5403, November 2013.

[10] R.D. Prabha and G.A. Rincon-Mora, "CMOS Photovoltaic-cell Layout Configurations for Harvesting Microsystems," *IEEE Int. Midwest Symp. on Circuits and Systems*, pp. 368–371, Aug. 2013.

[11] A.A. Blanco and G.A. Rincón-Mora, "Energy-Harvesting Microsensors: Low-Energy Task Schedule & Fast Drought-Recovery Design," *IEEE Midwest Symposium on Circuits and Systems*, Abu Dhabi, UAE, Oct. 16–19, 2016.

[12] J. Im, *et al.*, "A 40mV Transformer-reuse Self-startup Boost Converter with MPPT Control for Thermoelectric Energy Harvesting," *IEEE J. of Solid-State Circuits*, vol. 47, pp. 3055–3067, Dec 2012.

[13] A.A. Blanco and G.A. Rincón-Mora, "A 44–93 µs 250–400-mV 0.18-µm CMOS Starter for DC-Sourced Switched-Inductor Energy Harvesters," *IEEE Trans. on Circuits and Systems II*, vol. 61, pp. 1002–1006, December 2014.

[14] P. Weng, H. Tang, P. Ku, and L. Lu, "50 mV-Input Batteryless Boost Converter for Thermal Energy Harvesting," *IEEE J. of Solid-State Circuits*, vol. 48, pp. 1031–1041, April 2013.

[15] P. Chen, *et al.*, "An 80 mV Startup Dual-Mode Boost Converter by Charge-Pumped Pulse Generator and Threshold Voltage Tuned Oscillator with Hot Carrier Injection," *IEEE J. of Solid-State Circuits*, vol. 47, pp. 2554–2562, Nov 2012.

[16] K. Kadirvel, *et al.*, "A 330nA Energy-harvesting Charger with Battery Management for Solar and Thermoelectric Energy Harvesting," *IEEE Int. Solid-State Circuits Conf.*, pp. 106–107, Feb. 2012.